Arch. Metall. Mater. **71** (2026), 1, 277-286

DOI: https://doi.org/10.24425/amm.2026.157789

ZHAO YE[1,2*], YIXUAN ZHANG[1,2]

ACTIVITY PREDICTION BY MODIFIED MOLECULAR INTERACTION VOLUME MODEL IN Au-Sn BASED LIQUID ALLOYS

The Modified Molecular Interaction Volume Model (M-MIVM) was applied to predict component activities in Au-Sn based liquid alloys. Activity data from nine binary alloy systems (Au-Bi, Au-Cu, etc.) were fitted to predict activities in four ternary systems (Au-Bi-Sn, Au-Cu-Sn, Au-Sb-Sn, Au-Sn-Zn). M-MIVM demonstrated superior predictive capability over both the Molecular Interaction Volume Model (MIVM) and the Subregular Solution Model (SRSM), achieving highest fitting accuracy for binary systems and best experimental agreement for ternary systems. The model successfully constructed iso-activity curves for ternary Au-Bi-Sn liquid alloys at 800-1000 K.

Keywords: M-MIVM; Liquid alloy; Au-Sn; Au-Bi-Sn; Activity

1. Introduction

With increasing global emphasis on environmental protection, the adoption of lead-free solder in electronic packaging has become an inevitable trend [1-3]. Au-Sn based alloys are regarded as candidate systems for high-reliability solders due to their excellent wettability, creep resistance, and suitable melting point [4-6]. The thermodynamic properties of these multicomponent alloys, specifically component activities, directly influence phase equilibrium, interfacial reactions, and service performance [7,8]. Scholars predominantly employed the electromotive force method to determine the thermodynamic properties of Au-Sn based ternary alloys. This technique was applied specifically to measure the activity of Sn in the Au-Bi-Sn, Au-Cu-Sn, and Au-Sb-Sn systems, as well as the activity of Zn in the Au-Sn-Zn system [9-12].

Direct experimental measurement of activity coefficients in multicomponent alloys was resource-intensive, requiring high material and labor costs, and was thus generally impractical for routine applications. This rendered the use of thermodynamic models to predict alloy activity coefficients a viable alternative. The Molecular Interaction Volume Model (MIVM) was proposed by Tao and provided a thermodynamic framework for predicting the activity of components in liquid alloys [13]. Utilizing a limited number of parameters, the MIVM was proven to accurately predict the thermodynamic properties of multicomponent alloy systems, particularly lead-free solders [14-17]. Dai improved upon the MIVM and proposed the Modified Molecular Interaction Volume Model (M-MIVM) [18]. It demonstrated excellent accuracy and reliability in predicting the thermodynamic properties of solder alloy systems such as Ag–Cu–Sb, Sn–Ag–Cu, and In–Sn [19-22]. The Subregular Solution Model (SRSM), proposed by Hardy [23], represents an improvement over the Regular Solution Model. The model successfully constructed the pressure-dependent phase diagram of the alloy system, revealed the anomalous mixing entropy behavior, and accurately characterized the component activity and vacuum separation behavior of the multi-component system [24-26]. Furthermore, the CALPHAD method served as a mature computational thermodynamics approach. By establishing reliable thermodynamic databases, it effectively guided the composition design of multicomponent solder alloys [27-31]. In recent years, its integration with machine learning methodologies further enabled high-throughput screening, significantly enhancing the accuracy of phase diagram calculations [32-34].

This study employed the M-MIVM to fit the activities in binary systems (Au-Bi, Au-Cu, Au-Sb, Au-Sn, Au-Zn, Bi-Sn, Cu-Sn, Sb-Sn, Sn-Zn) and subsequently predict the activities in ternary liquid alloys (Au-Bi-Sn, Au-Cu-Sn, Au-Sb-Sn, Au-Sn-Zn). The predictions were systematically compared with

[1] SHANGHAI ZHONGQIAO VOCATIONAL AND TECHNICAL UNIVERSITY, SCHOOL OF ARCHITECTURAL ENGINEERING, SHANGHAI 201514, CHINA
[2] SHANGHAI ZHONGQIAO VOCATIONAL AND TECHNICAL UNIVERSITY, COMPUTATIONAL MATERIALS SCIENCE APPLICATION RESEARCH PLATFORM, SHANGHAI 201514, CHINA
* Corresponding author: yezhao@shzq.edu.cn

experimental data and results from both the original MIVM and SRSM models. The results demonstrated that M-MIVM achieved optimal performance in both fitting and prediction accuracy, establishing it as the currently superior activity prediction model. Using this model, iso-activity curves for all components in the ternary Au-Bi-Sn liquid alloy system at 800K were successfully constructed. Furthermore, the findings provide valuable references for the metallurgical design of Au-Sn based multicomponent alloys.

2. Methods

2.1. Molecular Interaction Volume Model

MIVM, proposed by Tao [13], was established based on the principles of statistical thermodynamics. In contrast to gas molecules that underwent continuous random motion and solid molecules that vibrated at fixed lattice sites, MIVM described liquid molecules as a medium migrating between cells in a non-random manner. For a multicomponent mixture, its molar excess Gibbs energy G_m^E can be generalized as

$$\frac{G_m^E}{RT} = \sum_{i=1}^{n} x_i \ln \frac{V_{mi}}{\sum_{j=1}^{n} x_j V_{mj} B_{ji}} - \frac{1}{2}\sum_{i=1}^{n} Z_i x_i \left(\frac{\sum_{j=1}^{n} x_j B_{ji} \ln B_{ji}}{\sum_{k=1}^{n} x_k B_{ki}} \right) \tag{1}$$

where x_i and V_{mi} are the molar function and molar volumes of component i, respectively; Z_i is the nearest molecules that construct a molecular cell or first coordination shell surrounding a center molecule i; n is the number of components; and B_{ij} and B_{ji} are pair-potential energy interaction parameters for an $i-j$ binary system and are defined, respectively, as

$$B_{ji} = \exp\left(-\frac{\varepsilon_{ji} - \varepsilon_{ii}}{kT} \right),\ B_{ij} = \exp\left(-\frac{\varepsilon_{ij} - \varepsilon_{jj}}{kT} \right) \tag{2}$$

where ε_{ii}, ε_{jj}, ε_{ij} and ε_{ji} are the pair-potential energy function of binary molecules of $i-i$, $j-j$, $i-j$ and $j-j$ respectively; k is Boltzmann's constant; and T is the temperature (K).

The coordination number of liquid pure component i can be defined as

$$Z_i = \frac{4\sqrt{2\pi}}{3} \left(\frac{r_{mi}^3 - r_{0i}^3}{r_{mi} - r_{0i}} \right) \rho_i r_{mi} \exp\left(\frac{\Delta H_{mi} \left(T_{mi} - T \right)}{Z_c R T T_{mi}} \right) \tag{3}$$

where $\rho_i = \dfrac{N_i}{V_i} = 0.6022 / V_{mi}$ is the molecular number density; $Z_c = 12$ is the close-packed coordination; ΔH_{mi} and T_{mi} are the melting enthalpy and temperature, respectively; R is the gas constant; T is the liquid metal temperature; and r_{0i} and r_{mi} are the beginning and first peak values of radial distance in a radial distribution function near the melting point, respectively.

An expression of the activity coefficient of component i can be deduced as

$$\ln \gamma_i = 1 + \ln \frac{V_{mi}}{\sum_{j=1}^{n} x_j V_{mj} B_{ji}} - \sum_{k=1}^{n} \frac{x_k V_{mi} B_{ik}}{\sum_{j=1}^{n} x_j V_{mj} B_{jk}} - \frac{1}{2}\left[\frac{Z_i \sum_{j=1}^{n} x_j B_{ji} \ln B_{ji}}{\sum_{l=1}^{n} x_l B_{li}} + \sum_{j=1}^{n} \frac{Z\ x_j B_{ij}}{\sum_{l=1}^{n} x_l B_{lj}} \times \left(\ln B_{ij} - \frac{\sum_{t=1}^{n} x_t B_{tj} \ln B_{tj}}{\sum_{l=1}^{n} x_l B_{lj}} \right) \right] \tag{4}$$

For a binary liquid mixture $i-j$, the expression of activity coefficients $\ln\gamma_i$ and $\ln\gamma_j$ can be expressed as

$$\ln \gamma_i = \ln\left(\frac{V_{mi}}{x_i V_{mi} + x_j V_{mj} B_{ji}} \right) + x_j \left(\frac{V_{mj} B_{ji}}{x_i V_{mi} + x_j V_{mj} B_{ji}} - \frac{V_{mi} B_{ij}}{x_j V_{mj} + x_i V_{mi} B_{ij}} \right) - \frac{x_j^2}{2} \left(\frac{Z_i B_{ji}^2 \ln B_{ji}}{\left(x_i + x_j B_{ji} \right)^2} + \frac{Z_j B_{ij} \ln B_{ij}}{\left(x_j + x_i B_{ij} \right)^2} \right) \tag{5}$$

$$\ln \gamma_j = \ln\left(\frac{V_{mj}}{x_j V_{mj} + x_i V_{mi} B_{ij}} \right) + x_i \left(\frac{V_{mj} B_{ji}}{x_i V_{mi} + x_j V_{mj} B_{ji}} - \frac{V_{mi} B_{ij}}{x_j V_{mj} + x_i V_{mi} B_{ij}} \right) - \frac{x_i^2}{2} \left(\frac{Z_j B_{ij}^2 \ln B_{ij}}{\left(x_j + x_i B_{ij} \right)^2} + \frac{Z_i B_{ji} \ln B_{ji}}{\left(x_i + x_j B_{ji} \right)^2} \right) \tag{6}$$

And the expression of activity coefficient of component 1 in ternary system is

$$\begin{aligned} \ln \gamma_1 = {} & 1 + \ln\left(\frac{V_{m1}}{x_1 V_{m1} + x_2 V_{m2} B_{21} + x_3 V_{m3} B_{31}} \right) \\ & - \frac{x_1 V_{m1}}{x_1 V_{m1} + x_2 V_{m2} B_{21} + x_3 V_{m3} B_{31}} \\ & - \frac{x_2 V_{m1} B_{12}}{x_1 V_{m1} B_{12} + x_2 V_{m2} + x_3 V_{m3} B_{32}} \\ & - \frac{x_3 V_{m1} B_{13}}{x_1 V_{m1} B_{13} + x_2 V_{m2} B_{23} + x_3 V_{m3}} \\ & - \frac{1}{2} \left(\frac{Z_1 \left(x_2 B_{21} + x_3 B_{31} \right) \left(x_2 B_{21} \ln B_{21} + x_3 B_{31} \ln B_{31} \right)}{\left(x_1 + x_2 B_{21} + x_3 B_{31} \right)^2} \right. \\ & + \frac{Z_2 x_2 B_{12} \left[\left(x_2 + x_3 B_{32} \right) \ln B_{12} - x_3 B_{32} \ln B_{32} \right]}{\left(x_1 B_{12} + x_2 + x_3 B_{32} \right)^2} \\ & \left. + \frac{Z_3 x_3 B_{13} \left[\left(x_2 B_{23} + x_3 \right) \ln B_{13} - x_2 B_{23} \ln B_{23} \right]}{\left(x_1 B_{13} + x_2 B_{23} + x_3 \right)^2} \right) \end{aligned} \tag{7}$$

2.2. Modified Molecular Interaction Volume Model

The M-MIVM adopted the cell model theory of the MIVM, which regarded the cells in liquid mixtures as carriers for molecular transfer. The most fundamental difference between the two lay in the fact that the MIVM utilized the molecular potential energy based on the quasi-lattice model, while the M-MIVM employed the average potential energy of mixtures derived from the Scatchard–Hildebrand theory. Based on the Scatchard–Hildebrand theory, Dai[18] assumed that the radial distribution function in the potential energy expression was a universal function independent of concentration, thereby establishing a new expression for the molecular interaction potential from a different perspective, which achieves separation between energy parameters and volume parameters. This formulation enabled the M-MIVM to simultaneously account for the contributions of both the microscopic configurational states (entropy) and molecular interactions (enthalpy) to the excess Gibbs free energy. The expression for the excess molar Gibbs energy G_m^E is

$$\frac{G_m^E}{RT} = -\sum_{i=1}^{C} x_i \ln\left(\sum_{j=1}^{C} x_j \frac{V_{mj}}{V_{mi}} B_{ji}\right) + \sum_{j>1}^{C}\sum_{i=1}^{C} x_i x_j \left(\frac{A_{ji}}{\sum_{l=1}^{C} x_l \frac{V_{ml}}{V_{mi}} B_{li}} + \frac{A_{ij}}{\sum_{l=1}^{C} x_l \frac{V_{ml}}{V_{mj}} B_{lj}}\right) \tag{8}$$

where C is the fraction of the component within the system; A_{ij} and A_{ji} are the energy parameters used to describe the interaction potential energy between molecules i and j, and are defined in Eq. (9); B_{ij} and B_{ji} are the volume parameters used to describe the volumetric changes of the system, and are defined in Eq. (10).

$$A_{ij} = \frac{K'}{T} C_j \left(\varepsilon_{ij} - \varepsilon_{jj}\right) = \frac{3K}{k} C_j^0 \left(\varepsilon_{ij} - \varepsilon_{jj}\right), \quad A_{ji} = \frac{K'}{T} C_i \left(\varepsilon_{ji} - \varepsilon_{ii}\right) = \frac{3K}{k} C_i^0 \left(\varepsilon_{ji} - \varepsilon_{ii}\right) \tag{9}$$

$$B_{ij} = \frac{P_{ij}}{P_{jj}},\ B_{ji} = \frac{P_{ji}}{P_{ii}} \tag{10}$$

Where C_i is a variable proportionality constant determined by temperature, and C_i^0 is a proportionality constant independent on temperature; K is a universal constant independent of the nature of the molecule and k is the Boltzmann constant; P_{ij} is the probability that the molecule i appears within the first coordination layer of the central molecule j.

An expression of the activity coefficient of component i can be deduced as

$$\ln\gamma_i = -\ln\left(\sum_{j=1}^{C} x_j D_{ji}\right) - \sum_{j=1}^{C} \frac{x_j}{\sum_{l=1}^{C} x_l D_{lj}} \left(D_{ij} - \sum_{l=1}^{C} x_l D_{lj}\right) + \sum_{j\neq i}^{C} x_j \left(\frac{A_{ji}}{\sum_{l=1}^{C} x_l D_{li}} + \frac{A_{ij}}{\sum_{l=1}^{C} x_l D_{lj}}\right) - \sum_{k>1}^{C}\sum_{j=1}^{C-1} x_j x_k \left(\frac{A_{kj}}{\sum_{l=1}^{C} x_l D_{lj}} + \frac{A_{jk}}{\sum_{l=1}^{C} x_l D_{lk}}\right) - \sum_{k>1}^{C}\sum_{j=1}^{C-1} x_j x_k \left[\frac{A_{kj}\left(D_{ij} - \sum_{t=1}^{C} x_t D_{tj}\right)}{\left(\sum_{l=1}^{C} x_l D_{lj}\right)^2} + \frac{A_{jk}\left(D_{ik} - \sum_{t=1}^{C} x_t D_{tk}\right)}{\left(\sum_{l=1}^{C} x_l D_{lk}\right)^2}\right] \tag{11}$$

Where $D_{ji} = B_{ji} V_{mj} / V_{mi}$.

For a binary alloy $i-j$, the expression of activity coefficients $\ln\gamma_i$ and $\ln\gamma_j$ can be defined in Eqs. (12) and (13), respectively.

$$\ln\gamma_i = -\ln\left(x_i + \frac{V_{mj}}{V_{mi}} B_{ji} x_j\right) - x_i x_j \left(\frac{1 - \frac{V_{mj}}{V_{mi}} B_{ji}}{x_i + \frac{V_{mj}}{V_{mi}} B_{ji} x_j}\right) - x_j^2 \left(\frac{\frac{V_{mi}}{V_{mj}} B_{ij} - 1}{x_j + \frac{V_{mi}}{V_{mj}} B_{ij} x_i}\right) + x_j^2 \left[\frac{A_{ji}}{x_i + \frac{V_{mj}}{V_{mi}} B_{ji} x_j} + \frac{A_{ij}}{x_j + \frac{V_{mi}}{V_{mj}} B_{ij} x_i}\right] - x_i x_j^2 \left[\frac{A_{ji}\left(1 - \frac{V_{mj}}{V_{mi}} B_{ji}\right)}{\left(x_i + \frac{V_{mj}}{V_{mi}} B_{ji} x_j\right)^2} + \frac{A_{ij}\left(\frac{V_{mi}}{V_{mj}} B_{ij} - 1\right)}{\left(x_j + \frac{V_{mi}}{V_{mj}} B_{ij} x_i\right)^2}\right] \tag{12}$$

$$\ln\gamma_j = -\ln\left(x_j + \frac{V_{mi}}{V_{mj}} B_{ij} x_i\right) - x_i x_j \left(\frac{1 - \frac{V_{mi}}{V_{mj}} B_{ij}}{x_j + \frac{V_{mi}}{V_{mj}} B_{ij} x_i}\right) - x_i^2 \left(\frac{\frac{V_{mj}}{V_{mi}} B_{ji} - 1}{x_i + \frac{V_{mj}}{V_{mi}} B_{ji} x_j}\right) + x_i^2 \left[\frac{A_{ji}}{x_i + \frac{V_{mj}}{V_{mi}} B_{ji} x_j} + \frac{A_{ij}}{x_j + \frac{V_{mi}}{V_{mj}} B_{ij} x_i}\right] - x_j x_i^2 \left[\frac{A_{ij}\left(1 - \frac{V_{mi}}{V_{mj}} B_{ij}\right)}{\left(x_j + \frac{V_{mi}}{V_{mj}} B_{ij} x_i\right)^2} + \frac{A_{ji}\left(\frac{V_{mj}}{V_{mi}} B_{ji} - 1\right)}{\left(x_i + \frac{V_{mj}}{V_{mi}} B_{ji} x_j\right)^2}\right] \tag{13}$$

And the expression of activity coefficient of component 1 in ternary system is

$$\begin{aligned}
\ln\gamma_1 &= -\ln\left(x_1 + x_2D_{21} + x_3D_{31}\right) \\
&-\frac{x_1}{x_1 + x_2D_{21} + x_3D_{31}}\left[1-\left(x_1 + x_2D_{21} + x_3D_{31}\right)\right] \\
&-\frac{x_2}{x_1D_{12} + x_2 + x_3D_{32}}\left[D_{12}-\left(x_1D_{12} + x_2 + x_3D_{32}\right)\right] \\
&-\frac{x_3}{x_1D_{13} + x_2D_{23} + x_3}\left[D_{13}-\left(x_1D_{13} + x_2D_{23} + x_3\right)\right] \\
&+x_2\left(\frac{A_{21}}{x_1 + x_2D_{21} + x_3D_{31}} + \frac{A_{12}}{x_1D_{12} + x_2 + x_3D_{32}}\right) \\
&+x_3\left(\frac{A_{31}}{x_1 + x_2D_{21} + x_3D_{31}} + \frac{A_{13}}{x_1D_{13} + x_2D_{23} + x_3}\right) \\
&-x_1x_2\left(\frac{A_{21}}{x_1 + x_2D_{21} + x_3D_{31}} + \frac{A_{12}}{x_1D_{12} + x_2 + x_3D_{32}}\right) \\
&-x_1x_3\left(\frac{A_{31}}{x_1 + x_2D_{21} + x_3D_{31}} + \frac{A_{13}}{x_1D_{13} + x_2D_{23} + x_3}\right) \\
&-x_2x_3\left(\frac{A_{32}}{x_1D_{12} + x_2 + x_3D_{32}} + \frac{A_{23}}{x_1D_{13} + x_2D_{23} + x_3}\right) \\
&-x_1x_2\left\{\begin{array}{l}\dfrac{A_{21}\left[1-\left(x_1 + x_2D_{21} + x_3D_{31}\right)\right]}{\left(x_1 + x_2D_{21} + x_3D_{31}\right)^2} \\ +\dfrac{A_{12}\left[D_{12}-\left(x_1D_{12} + x_2 + x_3D_{32}\right)\right]}{\left(x_1D_{12} + x_2 + x_3D_{32}\right)^2}\end{array}\right\} \\
&-x_1x_3\left\{\begin{array}{l}\dfrac{A_{31}\left[1-\left(x_1 + x_2D_{21} + x_3D_{31}\right)\right]}{\left(x_1 + x_2D_{21} + x_3D_{31}\right)^2} \\ +\dfrac{A_{13}\left[D_{13}-\left(x_1D_{13} + x_2D_{23} + x_3\right)\right]}{\left(x_1D_{13} + x_2D_{23} + x_3\right)^2}\end{array}\right\} \\
&-x_2x_3\left\{\begin{array}{l}\dfrac{A_{32}\left[D_{12}-\left(x_1D_{12} + x_2 + x_3D_{32}\right)\right]}{\left(x_1D_{12} + x_2 + x_3D_{32}\right)^2} \\ +\dfrac{A_{23}\left[D_{13}-\left(x_1D_{13} + x_2D_{23} + x_3\right)\right]}{\left(x_1D_{13} + x_2D_{23} + x_3\right)^2}\end{array}\right\}
\end{aligned} \tag{14}$$

2.3. Subregular Solution Model

The well-known SRSM has been extensively used for over 70 years [23]. In this model, the molar excess Gibbs energy of the $i-j$ binary system is simply given by

$$G_m^E / RT = x_ix_j(A_{ij}x_i + A_{ji}x_j) \tag{15}$$

Where A_{ij} and A_{ji} are constants related to temperature. Thus, the activity coefficients of both components in the system can be expressed as, respectively,

$$\ln\gamma_i = x_j^2\left[2A_{ij}x_i + A_{ji}(x_j - x_i)\right] \tag{16}$$

$$\ln\gamma_j = x_i^2\left[2A_{ij}x_j + A_{ij}(x_i - x_j)\right] \tag{17}$$

If the SRSM is obeyed by all the binary systems, the molar excess Gibbs energy of the Chou model[35] for ternary system can be generalized as

$$\begin{aligned}
G_i^E &= G^E + (\partial G^E / \partial x_i)_{x[i,k]} \\
&-\sum x_j(\partial G^E / \partial x_i)_{x[j,k]}(j = 1 \sim k-1)
\end{aligned} \tag{18}$$

and the expression of activity coefficient of component 1 is

$$\begin{aligned}
\ln\gamma_{1[temary]} &= (x_2^2 + x_2x_3\xi_{2(12)}^{(3)}) / (x_2 + x_3\xi_{2(12)}^{(3)})^2 \ln\gamma_{1(12)} \\
&+ x_2x_3\xi_{1(12)}^{(3)} / (x_1 + x_3\xi_{1(12)}^{(3)})^2 \ln\gamma_{2(12)} \\
&- x_2x_3\xi_{3(23)}^{(1)} / (x_3 + x_1\xi_{3(23)}^{(1)})^2 \ln\gamma_{2(23)} \\
&- x_2x_3\xi_{2(23)}^{(1)} / (x_2 + x_1\xi_{2(23)}^{(1)})^2 \ln\gamma_{3(23)} \\
&+ (x_3^2 + x_2x_3\xi_{3(13)}^{(2)} / (x_3 + x_2\xi_{3(13)}^{(2)})^2 \ln\gamma_{1(13)} \\
&+ x_2x_3\xi_{1(13)}^{(2)} / (x_1 + x_2\xi_{1(13)}^{(2)})^2 \ln\gamma_{3(13)}
\end{aligned} \tag{19}$$

Where $\xi_{i(ij)}^{(k)}$ is the similar coefficient and:

$$\xi_{i(ij)}^{(k)} = \eta(ij,ik) / \left[\eta(ij,ik) + \eta(ji,jk)\right],$$

$$\eta(ij,ik) = \int\left(\Delta G_{ij}^E - \Delta G_{ik}^E\right)^2 dx_i\Delta G_{ij}^E .$$

3. Results and discussion

3.1. Prediction of activities of binary alloy systems

The related parameters of pure matter components for MIVM and M-MIVM are used to calculate V_{mi} and Z_i, and are listed in TABLE 1.

According to Eqs. (5) and (6), the B_{ij} and B_{ji} values of MIVM are obtained by fitting their component activities [37]. When the infinite dilute activity coefficients are known, the B_{ij} and B_{ji} values of MIVM of the binary liquid alloys can be determined by using the Newton-Raphson methodology. Similarly, the B_{ij} and B_{ji} values and the A_{ij} and A_{ji} values of M-MIVM can be determined using Eqs. (12) and (13). For SRSM, the A_{ij} and A_{ji} values can be determined using Eqs. (16) and (17). All associated parameters for these models are listed in TABLE 2.

To characterize the deviations between the experimental values and calculated data accurately, the average standard deviations S_i^* and average relative deviations S_i of each model were calculated using Eq. (20), as shown in TABLE 2.

$$\begin{aligned}
S_i^* &= \pm\left[\frac{1}{m}\sum_{i=1}^{m}\left(a_{i,\exp} - a_{i,pre}\right)^2\right]^{1/2}, \\
S_i &= \pm\frac{100}{m}\sum_{i=1}^{m}\left|\frac{a_{i,\exp} - a_{i,pre}}{a_{i,\exp}}\right|
\end{aligned} \tag{20}$$

where $a_{i,\exp}$ and $a_{i,pre}$ are the experimental data and the predicted values of activity of component$i$, respectively; m is the number of experimental data.

TABLE 1

Related parameters of pure components for MIVM and M-MIVM[36]

i	V_{mi} (cm^3/mol)	ΔH_{mi} (kJ/mol)	r_{mi} (10^{-8}cm)	r_{0i} (10^{-8}cm)
Au	$11.37[1 + 0.69 \times 10^{-4}(T - 1337)]$	12.76	2.88	2.46
Bi	$20.87[1 + 1.17 \times 10^{-4}(T - 544)]$	10.88	3.38	2.68
Cu	$7.99[1 + 1.0 \times 10^{-4}(T - 1311)]$	13	2.56	2.15
Sb	$18.87[1 + 1.3 \times 10^{-4}(T - 904)]$	39.7	3.14	2.57
Sn	$17.03[1 + 0.87 \times 10^{-4}(T - 505)]$	7.07	3.16	2.59
Zn	$9.99[1 + 1.5 \times 10^{-4}(T - 693)]$	7.28	2.79	2.30

TABLE 2

Part of the parameters of MIVM, M-MIVM and SRSM in binary liquid alloys

System		MIVM				M-MIVM						SRSM			
$i-j$	T (K)	B_{ij}	B_{ji}	S^*	S	A_{ij}	A_{ji}	B_{ij}	B_{ji}	S^*	S	A_{ij}	A_{ji}	S^*	S
Au-Bi	1400	0.72	1.222	0.0079	11.41	–0.249	–0.213	2.1	0.508	0.0073	11.26	–0.52	–0.52	0.0073	11.26
Au-Cu	1550	1.915	0.367	0.0094	11.42	–0.96	–0.96	0.67	1.34	0.0003	9.24	–1.87	–1.87	0.0003	9.22
Au-Sb	1400	1.58	0.92	0.0097	11.70	–0.25	–0.25	4.5	0.85	0.0073	11.57	–1.63	–2.15	0.0120	12.49
Au-Sn	823	1.15	2	0.0094	9.47	–3.1	–4.37	0.8	1.15	0.0068	9.44	–9.6	–5.15	0.0132	9.70
Au-Zn	1080	1.79	1.798	0.0515	19.71	–4	–5.3	0.89	1.21	0.0334	16.64	–9.62	–8.895	0.0342	14.95
Bi-Sn	600	1.095	0.856	0.0003	9.15	–0.232	0.136	0.704	1.022	0.0002	9.13	0.18	0.248	0.0002	9.13
Cu-Sn	1400	0.652	1.599	0.0666	29.22	–1.89	–0.37	0.55	0.12	0.0066	10.94	–3.7	–0.3	0.0440	21.75
Sb-Sn	905	1.0779	1.0947	0.0003	9.23	–0.473	–0.473	0.9	1.032	0.0002	9.20	–0.892	–0.892	0.0002	9.20
Sn-Zn	750	1.1202	0.6155	0.0021	9.37	–0.36	–0.07	0.41	0.172	0.0014	9.28	0.58	1.315	0.0084	10.26
Overall mean				0.0175	13.41					0.0071	10.74			0.0133	12.00

From Table 2, it can be seen that M-MIVM exhibits the smallest S^* and S among the three models, indicating its superior fitting capability. M-MIVM not only surpasses its prototype MIVM, but also outperforms SRSM, which is renowned for its excellent binary fitting performance. A reasonable explanation for the aforementioned results is that, compared to the two adjustable parameters models MIVM and SRSM, M-MIVM incorporates four adjustable parameters, enabling it to surpass the fitting capability limits of its predecessors and achieve a new level of performance. For instance, in the Cu–Sn system at 1400 K, the S^* and S of M-MIVM were 0.0066 and 10.94%, respectively, significantly lower than those of MIVM (0.0666 and 29.22%) and SRSM (0.0440 and 21.75%). However, this does not imply that M-MIVM achieves perfect fitting for all systems, as it still exhibits limitations, with the Au–Zn system at 1080 K serving as an example.

3.2. Prediction of activities of ternary systems

The MIVM, M-MIVM, and SRSM were employed to predict the activities of Sn in ternary liquid systems Au-Bi-Sn, Au-Cu-Sn, Au-Sb-Sn and Zn in the Au-Sn-Zn system, with systematic comparisons made against experimental data as presented in TABLE 3.

TABLE 3 reveals discrepancies between the model-predicted and experimentally measured activities of Sn in the ternary liquid alloys Au-Bi-Sn, Au-Cu-Sn, Au-Sb-Sn, and Zn in Au-Sn-Zn. The MIVM exhibits significant predictive deviations, with mean S^* and S reaching 0.0430 and 18.22%, respectively, across these four systems. The SRSM shows slightly better performance, with S^* and S values of 0.0368 and 23.02%, respectively. In contrast, the M-MIVM demonstrates the best agreement, achieving S^* and S as low as 0.0285 and 11.55%,

TABLE 3

The average standard deviations S^* and average relative deviations S of MIVM, M-MIVM and SRSM

Systems		MIVM		M-MIVM		SRSM	
$i-j$	T (K)	S^*	S	S^*	S	S^*	S
Au-Bi-Sn [9]	800	0.0093	14.55	0.0079	4.53	0.0121	12.23
Au-Cu-Sn [10]	1273	0.0797	18.90	0.0671	15.86	0.0913	31.42
Au-Sb-Sn [11]	873	0.0245	19.12	0.0144	11.64	0.0169	18.45
Au-Sn-Zn [12]	973	0.0586	20.30	0.0246	14.18	0.0269	29.97
Overall mean		0.0430	18.22	0.0285	11.55	0.0368	23.02

respectively. Notably, the M-MIVM consistently yields the smallest deviations between predicted and experimental values in both metrics, demonstrating its superior predictive accuracy and reliable stability. However, although the predictive accuracy of the M-MIVM for the activity of Sn in the Au–Cu–Sn system at 1273 K is superior to that of the MIVM and SRSM, its results still exhibit significant deviations from the experimental values.

To complement the microscopic analysis, Fig. 1 provides a detailed visualization of the prediction errors between the model-calculated values and experimental data. The comparative analysis confirms that M-MIVM demonstrates superior predictive performance even at the microscopic level, exhibiting both high reliability and stability in its predictions.

Fig. 1(a) shows that for the Au-Bi-Sn liquid ternary system at 800 K, the predicted values of activities of Sn from the three models are generally consistent on a global scale and agree well with the experimental data.

Fig. 1(b) shows that for the Au-Cu-Sn liquid ternary system at 1273 K, the predicted values from all models are significantly lower than the experimental data points, indicating a systematic underestimation of the activity of Sn. This strong systematic negative deviation may originate from certain strong interactions present in the binary systems that are not fully captured in the ternary environment. Nevertheless, M-MIVM exhibits the slightest degree of underestimation, demonstrating its superior corrective capability. However, in the Sn-rich region ($a_{Sn} > 0.75$), SRSM unexpectedly outperforms M-MIVM, possibly due to the stronger non-ideality and asymmetric interactions that are not fully accounted for in M-MIVM's current parameterization.

Fig. 1(c) shows that for the Au-Sb-Sn liquid ternary system at 873 K, the M-MIVM predictions match the experimental values most accurately, whereas the other two models exhibit relatively larger deviations. Notably, the MIVM exhibits a significant systematic positive deviation, with its predicted values

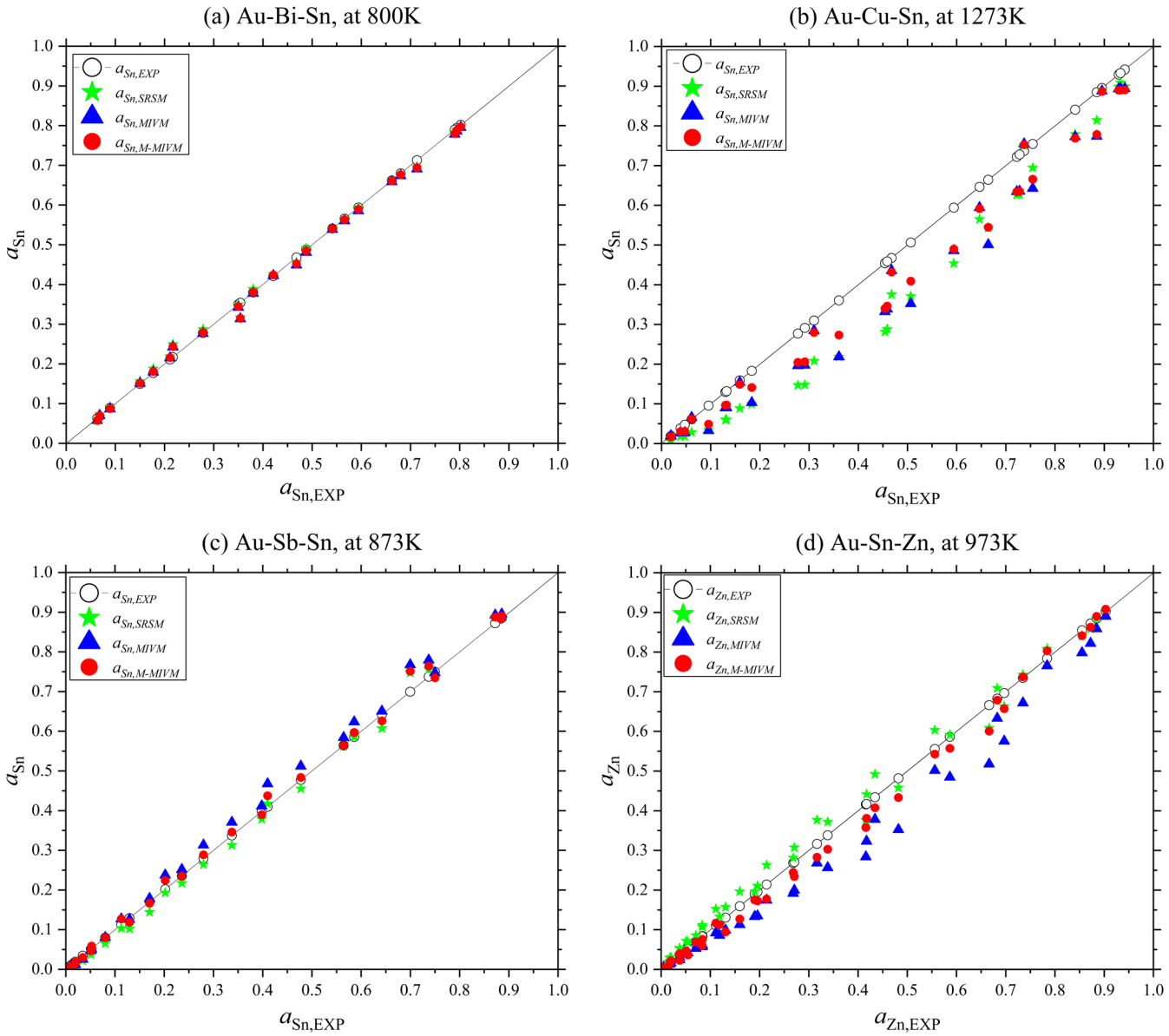

Fig. 1. Prediction values and experimental data of activities: (a) Sn in ternary Au-Bi-Sn liquid alloys at 800 K [9]; (b) Sn in ternary Au-Cu-Sn liquid alloys at 1273 K [10]; (c) Sn in ternary Au-Sb-Sn liquid alloys at 873 K [11]; (d) Zn in ternary Au-Sn-Zn liquid alloys at 973 K [12]

lying above the experimental data points throughout the entire concentration range, indicating a consistent overestimation of tin activity. In contrast, the SRSM demonstrates a systematic slight negative deviation, with most of its predicted values located below the experimental data points. The M-MIVM performs most optimally, showing the closest agreement between its predicted values and the experimental data points.

Fig. 1(d) shows that for the Zn activities in the Au-Sn-Zn liquid ternary system at 973 K, the M-MIVM predictions again show the highest consistency with experimental data, followed by SRSM, while MIVM performs the worst. It is also noted that both MIVM and M-MIVM predictions exhibit negative deviations relative to the experimental values, whereas SRSM predictions show positive deviations, indicating that MIVM and M-MIVM share a common theoretical origin and exhibit consistent prediction trends.

The superior performance of M-MIVM can be attributed to the following reasons: 1. M-MIVM inherits the solid physical foundation of MIVM, which provides a theoretical basis for predicting multicomponent liquid alloys; 2. The reasonable assumptions based on Scatchard-Hildebrand theory endow M-MIVM with enhanced fitting and predictive capabilities; 3. The predictive accuracy for multicomponent systems fundamentally depends on the fitting performance of their constituent binary systems. This principle holds universally across thermodynamic models. Consequently, the enhanced fitting capability attained through the four parameters design leads to a substantial improvement in predictive performance.

3.3. Prediction of activities of all components in ternary Au-Bi-Sn lead-free solders

The activities of components in the Au-Bi-Sn ternary liquid alloy were predicted using the M-MIVM, with the corresponding iso-activity curves plotted as shown in Figs. 2-4.

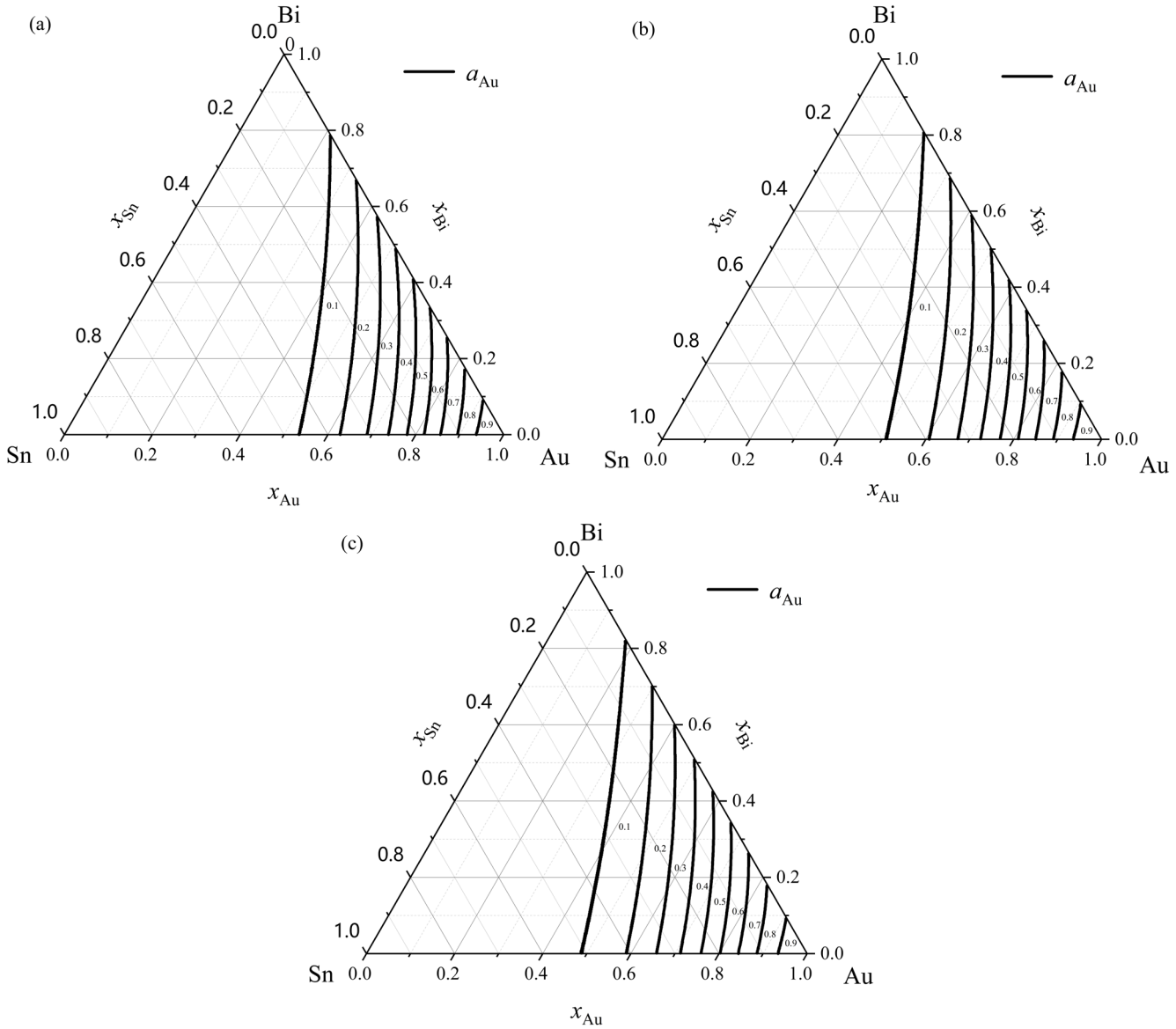

Fig. 2. Iso-activity curves from 0.1 to 0.9 of Au in ternary Au-Bi-Sn lead-free solders: (a) Iso-activity curves at 800 K; (b) Iso-activity curves at 900 K; (c) Iso-activity curves at 1000 K

Fig. 2(a)-(c) shows that the activity of Au in the ternary system exhibits significant negative deviations from Raoult's law, with the deviation magnitude decreasing as the x_{Bi}/x_{Sn} ratio increases. This indicates that as the Bi content increases, the strong interaction between Au and Sn is weakened, thereby reducing the activity of Au. Additionally, within the temperature range of 800-1000 K, the a_{Au} value for the same composition on any cross-section increases with rising temperature.

Fig. 3(a)-(c) demonstrates that the positive deviation of a_{Bi} initially increases then decreases with rising x_{Au}/x_{Sn} ratio, eventually transitioning to negative deviation. Particularly noteworthy is that the transition point composition remains relatively constant ($x_{Sn} \approx 0.07$ when $a_{Bi} \leq 0.6$) despite variations in activity of Bi. Also, the figures indicates that as temperature increases, the deviation of a_{Bi} from Raoult's law decreases at any given cross-section. However, this trend is not particularly evident in the bismuth-rich region.

Fig. 4(a)-(c) reveals that the activity of Sn in the ternary system exhibits significant negative deviations from Raoult's law. These deviations weaken as the x_{Bi}/x_{Au} ratio increases and ultimately transition into slight positive deviations. In addition, a_{Sn} increases with rising temperature across all cross-sections. Similarly, this trend is not distinctly observed in the Sn-rich region.

4. Conclusion

A systematic analysis of the thermodynamic properties of Au-Sn based liquid alloys was conducted through the Modified Molecular Interaction Volume Model (M-MIVM). Compared to the MIVM and SRSM, this model demonstrated the highest accuracy in fitting binary systems and the best performance in predicting ternary systems. The successfully constructed iso-activity curves for the Au-Bi-Sn ternary system at 800-1000 K

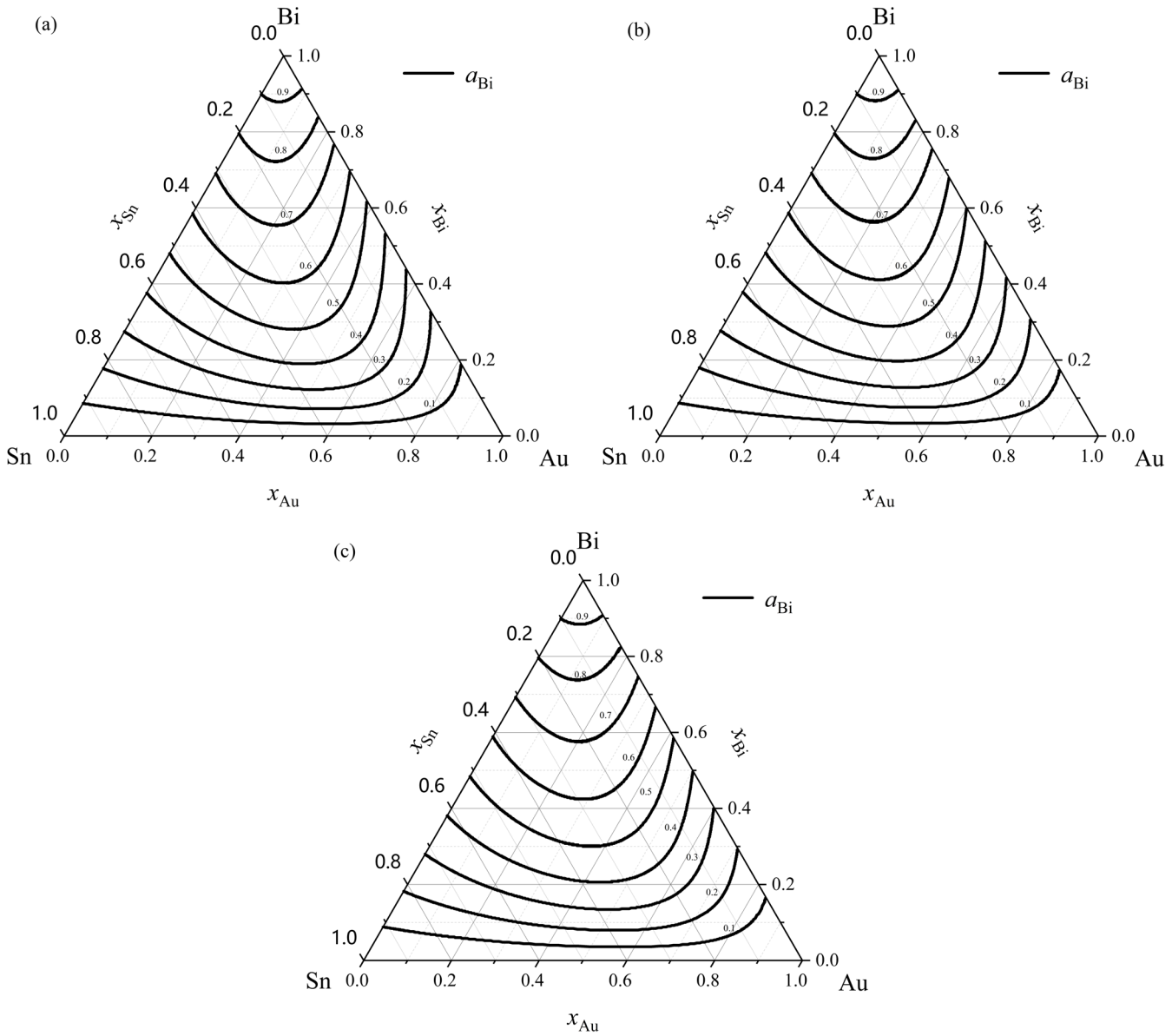

Fig. 3. Iso-activity curves from 0.1 to 0.9 of Bi in ternary Au-Bi-Sn lead-free solders: (a) Iso-activity curves at 800 K; (b) Iso-activity curves at 900 K; (c) Iso-activity curves at 1000 K

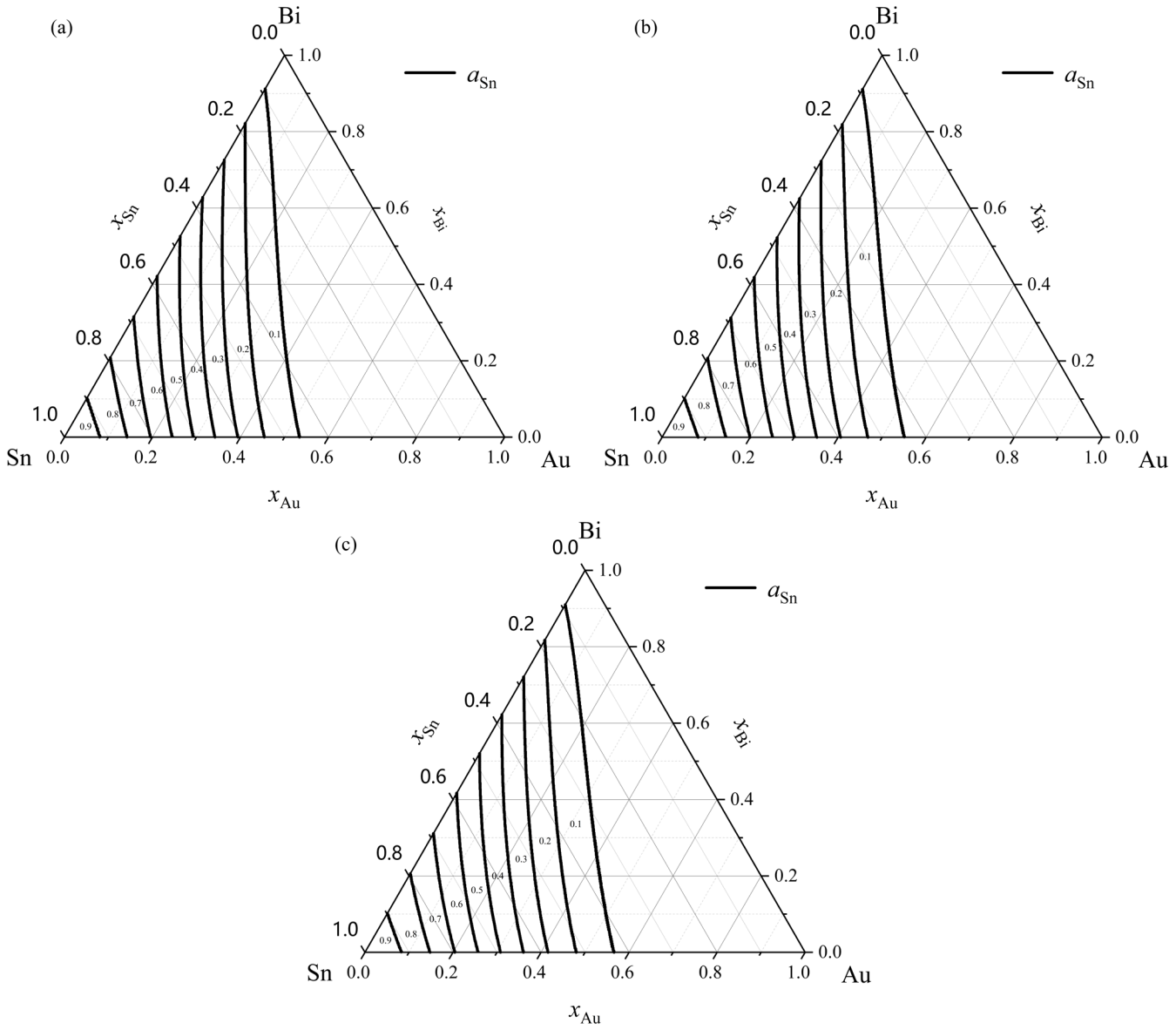

Fig. 4. Iso-activity curves from 0.1 to 0.9 of Sn in ternary Au-Bi-Sn lead-free solders: (a) Iso-activity curves at 800 K; (b) Iso-activity curves at 900 K; (c) Iso-activity curves at 1000 K

clearly revealed the activity variation patterns of each component. These results contribute to a more comprehensive understanding of Au-Sn based lead-free solder systems and provide a theoretical foundation for the metallurgical design of similar types of lead-free solders.

However, it should be noted that the M-MIVM also exhibits certain limitations. For instance, the model is sensitive to input parameters (such as energy and volume parameters), which may affect the stability of prediction results. Additionally, the computational demand increases significantly when dealing with multicomponent systems, potentially limiting its application in high-throughput calculations.

Future research will focus on further optimizing the parameter acquisition process of M-MIVM and enhancing its predictive accuracy. Moreover, coupling M-MIVM with the CALPHAD method represents a promising direction, facilitating the design of multicomponent alloy systems with tailored properties.

Acknowledgements

This work is financially supported by Research Project of Shanghai Zhongqiao Vocational and Technical University, China (Grant No. 2025ZQZR56).

REFERENCE

[1] M. Abtew, G. Selvaduray, Materials Science and Engineering: R: Reports **27**, 95 (2000).

[2] K. Zeng, K.N. Tu, Materials Science and Engineering: R: Reports **38**, 55 (2002).

[3] K. Suganuma, Current Opinion in Solid State and Materials Science **5**, 55 (2001).

[4] G. Zeng, S. McDonald, K. Nogita, Microelectronics Reliability **52**, 1306 (2012).

[5] C.J. Müller, V. Bushlya, M. Ghasemi, S. Lidin, M. Valldor, F. Wang, J. Mater. Sci. **50**, 7808 (2015).
[6] X. Wang, L. Zhang, M. Li, Mater. Trans. **63**, 93 (2022).
[7] J. Tomiska, Thermochimica Acta **314**, 145 (1998).
[8] D. Adhikari, R.P. Koirala, B.P. Singh, Nepal Journals, Bibechana (2013).
[9] Z. Guo, W. Yuan, M. Hindler, A. Mikula, The Journal of Chemical Thermodynamics **48**, 201 (2012).
[10] Z. Guo, M. Hindler, W. Yuan, A. Mikula, Thermochimica Acta **525**, 183 (2011).
[11] M. Hindler, Z. Guo, A. Mikula, The Journal of Chemical Thermodynamics **55**, 102 (2012).
[12] S. Karlhuber, A. Mikula, F. Sommer, Metall. Mater. Trans. B **27**, 921 (1996).
[13] D.P. Tao, Thermochimica Acta **363**, 105 (2000).
[14] S.K. San, I. Koirala, J. Phys. Commun. **7**, 105001 (2023).
[15] L.-M. Liang, G.-H. Ding, Y.-X. Wang, Y. Liu, Physics and Chemistry of Liquids **59**, 706 (2021).
[16] S.K. Sah, R.P. Chaudhary, M.K. Jha, I. Koirala, I.S. Jha, Welding International **38**, 823 (2024).
[17] S.K. Sah, I.S. Jha, I. Koirala, Welding International **38**, 265 (2024).
[18] H. Dai, D.P. Tao, Fluid Phase Equilibria **473**, 154 (2018).
[19] Q. Li, Y. Tian, L. Kong, B. Yang, B. Xu, W. Jiang, L. Wang, Metals **14**, 603 (2024).
[20] Y. You, L. Kong, J. Xu, B. Xu, G. Liu, B. Yang, Results in Chemistry **3**, 100143 (2021).
[21] J. Pang, H. Wu, L. Kong, J. Xu, B. Xu, B. Yang, Separation and Purification Technology **330**, 125166 (2024).
[22] Y. You, J. Xu, L. Kong, B. Xu, B. Yang, Mater. Res. Express **8**, 096508 (2021).
[23] H.K. Hardy, Acta Metallurgica **1**, 202 (1953).
[24] S. Ben Shalom, H.G. Kim, M. Emuna, U. Argaman, Y. Greenberg, J. Lee, E. Yahel, G. Makov, Journal of Alloys and Compounds **822**, 153537 (2020).
[25] A. Takeuchi, Mater. Trans. **61**, 1717 (2020).
[26] Q. Li, Y. Tian, L. Kong, B. Yang, B. Xu, W. Jiang, L. Wang, Metals **14**, 603 (2024).
[27] M. Li, M.H. Rong, Y. Wu, P.F. Tan, J. Wang, Calphad **90**, 102859 (2025).
[28] Q. Zhang, H. Chen, Q. Luo, Y. Yuan, H. Liu, Q. Li, J. Mater. Sci. **57**, 6819 (2022).
[29] D. Cui, J. Wang, N. Yan, J. Phase Equilib. Diffus. **43**, 214 (2022).
[30] Y. Bai, Q. Tong, M. Rong, C. Tan, X. Liu, M. Li, J. Wang, Materials **17**, 2137 (2024).
[31] X. Luo, J. Peng, W. Zhang, S. Wang, S. Cai, X. Wang, Materials Science and Engineering: A **860**, 144284 (2022).
[32] A. Sundar, X. Tan, S. Hu, M.C. Gao, Journal of Materials Research **40**, 112 (2025).
[33] S. Zhu, R. Arróyave, D. Sarıtürk, Acta Materialia **286**, 120747 (2025).
[34] Y. Zeng, M. Man, C. Koon Ng, Z. Aitken, K. Bai, D. Wuu, J. Jun Lee, S. Rong Ng, F. Wei, P. Wang, D. Cheng Cheh Tan, Y.-W. Zhang, Materials & Design **241**, 112929 (2024).
[35] K.-C. Chou, S.-K. Wei, Metall. Mater. Trans. B **28**, 439 (1997).
[36] T. Iida, R.I.L. Guthrie, *T*he Physical Properties of Liquid Metals (Clarendon Press, Oxford, 1988).
[37] R. Hultgren, P.D. Desai, D.T. Hawkins, M. Gleiser, K.K. Kelley, Selected Values of the Thermodynamic Properties of Binary Alloys (American Society for Metals, Metals Park, Ohio, 1973).